21st Australasian Fluid Mechanics Conference
Adelaide, Australia
10-13 December 2018

Receptivity analysis in under-expanded supersonic impinging jets

Shahram Karami[1], Paul Stegeman[1], Andrew Ooi [2], Vassilis Theofilis [3] and Julio Soria[1]

[1] Laboratory for Turbulence Research in Aerospace & Combustion (LTRAC), Department of Mechanical and Aerospace Engineering
Monash University, Victoria 3800, Australia

[2] Department of Mechanical Engineering
University of Melbourne, Victoria 3010, Australia

[3] School of Engineering
University of Liverpool, Liverpool, L69 7ZX, UK

Abstract

This paper presents the receptivity process at the nozzle-lip to an external forcing in the configuration of under-expanded supersonic impinging jets. The nozzle-lip is considered as a linear transformer. Therefore, the linearised three-dimensional Navier Stokes equations in cylindrical coordinate are considered. The mean flow fields are obtained from large-eddy simulations. An impulse response analysis of the linearised system is performed which allows a wide range of frequencies to be excited. The transfer function at the nozzle-lip is used to characterise the receptivity process. The sensitivity of the transfer function to the pulse location and the azimuthal wave number is performed.

It is found that external forces at the vicinity of the infinite lip and with Strouhal numbers in the ranges of 0.7 to 6.5 have the highest amplification. This is consistent for all the azimuthal wave numbers in the nozzle-to-wall distance of $2d$ but not for the azimuthal wave number two for the nozzle-to-wall distance of $5d$. For this case, external forces located at angles between 15° and 50° from the jet centreline also have high amplification in contrast to the nozzle-to-wall distance of $2d$. Based on these results, the region close to the infinite lip is found to be a prominent candidate to control instabilities in this configuration.

Introduction

The under-expanded jets which form when the static pressure at the nozzle exit is higher than the ambient pressure, occur in engineering applications such as an exhaust of aircraft and rockets, mixing process in supersonic combustors and accidental leakage of pressurized fluid. An impingement is inevitable in the short take-off and landing aircrafts. The impingement adds complexity to this very enriched flow. An acoustic-hydrodynamic instability is known to cause self-sustained oscillations in this configuration. These oscillations of the flow have been observed in subsonic impinging jets [6], a resonance tube, an edge-tone and a plate with cavity [16]. The feedback loop analogy of Powell [15] is the main existing and commonly accepted theory explaining these oscillations. The feedback loop is based on interactions of the sound and the jet flow. The shear-layer disturbances develop in the form of Kelvin-Helmholtz instabilities and interact with the oblique shock, Mach disk and stand-off shock. These interactions displace the shocks which creates high-intensity acoustic waves at the shock locations and the impingement. These acoustic waves travel upstream. As the boundary of the jet is expanded upon exit from the nozzle, some or all of these acoustic waves might be blocked. These waves are also reflected by the surrounding structures. Either the reflected waves from the surrounding surfaces or upstream propagation waves, reach the nozzle lip and by perturbing the shear layer at nozzle lip close the feedback loop. The appearance of coherent structures in the shear layer of the jet and their downstream convection have been observed in many experimental and numerical studies of impinging under-expanded supersonic jets [15, 1, 4]. A prevailing belief is that the acoustic waves scattered by the nozzle lip through the receptivity process internalise as shear layer Kelvin Helmholtz instabilities and form these coherent structures [10, 5, 15, 9]. Receptivity is defined as the process of shear layer instabilities being excited by external disturbances and has been studied since 1970's. A vortex-sheet model of infinite extent was commonly used to study the receptivity of trailing edge of the splitter plate [7, 2, 12]. Despite the restriction of the model to a band of low frequencies [3], it provides useful qualitative information. The physical interpretation of the excitation of the shear layer by acoustic waves is presented by Tam [18] where it was stated that the overlap of the spatial and temporal wavenumbers of the acoustic waves and the shear layer instabilities is a condition required for receptivity.

The previous studies have mainly focused on receptivity in a rather simple configuration of mixing layer formed by splitter plate. There is very little study of the receptivity in self-excited jet flows and to the best of our knowledge, there is even less study on receptivity in under-expanded supersonic jets. There have been numerous experimental and numerical studies of supersonic impinging jets; however, these studies have only focused on large coherent structures and far too little attention has been paid to the mechanism by which these structures are initialised. Therefore, the primary objective of this paper is to fill this gap by analysing the receptivity process in the under-expanded supersonic impinging jets.

Problem formulation and numerical methods

Governing equations

The compressible conservation equations of mass, momentum, and total energy in cylindrical coordinates are the governing equations that apply to supersonic under-expanded impinging jets. These equations are non-dimensionalised with respect to the ambient conditions. The linearised Navier Stokes equations (LNSE) are derived by superimposing small amplitude disturbances on a mean flow. Denoting the mean flow variables as $\overline{(\ldots)}$ and perturbations as $(\ldots)'$, the linearised Navier Stokes equations are given as

$$\frac{\partial \rho'}{\partial t} = -\nabla\cdot(\rho\mathbf{u})', \tag{1}$$

$$\frac{\partial (\rho\mathbf{u})'}{\partial t} = -\nabla\cdot\left(\overline{\rho\mathbf{u}}\otimes\mathbf{u}' + (\rho\mathbf{u})'\otimes\overline{\mathbf{u}}\right) - \nabla p' + \overline{\mu}\nabla\cdot\mathbb{T}' \tag{2}$$

$$\frac{\partial (\rho e)'}{\partial t} = -\nabla\cdot\left(\overline{(\rho e+p)}\mathbf{u}' + (\rho e+p)'\overline{\mathbf{u}}\right) + \overline{k}\nabla^2 T' + \overline{\mu}V_{KE}, \tag{3}$$

where

$$V_{KE} = \left((\nabla\cdot\mathbb{T}')\cdot\overline{\mathbf{u}}+(\nabla\cdot\mathbb{T}')\cdot\mathbf{u}'+\mathbb{T}':\nabla\overline{\mathbf{u}}+\overline{\mathbb{T}}:\nabla\mathbf{u}'\right) \quad (4)$$

$$\mathbb{T} = \nabla\mathbf{u}+(\nabla\mathbf{u})^T+\left(\frac{\mu_B}{\mu}-\frac{2}{3}\right)(\nabla\cdot\mathbf{u})\mathbb{I},$$

$$(\rho e)' = \frac{1}{2}\rho\|\mathbf{u}'\|^2+\frac{p'}{\gamma-1},$$

and the linearised version of the equation of state is

$$p' = \frac{\overline{\rho}T'+\rho'\overline{T}}{M_0^2}. \quad (5)$$

Finally, the viscosity and thermal conductivity are given by

$$\overline{\mu} = \frac{\overline{T}^{0.76}}{Re} \quad \text{and} \quad \overline{k} = \overline{\mu}\frac{\gamma}{\gamma-1}\frac{1}{M_0^2 Pr}. \quad (6)$$

These equations are commonly presented in the concise matrix form

$$\frac{\partial q'}{\partial t} = \mathbb{A}q', \quad (7)$$

where q' is the perturbations $(\rho', u_x', u_r', u_\theta', e')$, and $\mathbb{A}$ is the linear operator advancing the small perturbation in time.

Configurations and numerical method

The configuration is an under-expanded impinging jet with nozzle–to–wall distances of $h = 2d$ and $5d$ where d is the jet diameter. The size of the domain in radial direction is $12d$. The mean inlet axial velocity U_{in} is specified using the hyperbolic-tangent function given by

$$\frac{U_{in}}{U_j} = \frac{1}{2}\left(1-\tanh\left[\frac{1}{4\delta_{in}}\left(\frac{r}{r_j}-\frac{r_j}{r}\right)\right]\right), \quad (8)$$

where U_j is the jet inlet velocity, r_j the jet inlet radius and δ_{in} the inlet momentum thickness. The inlet momentum thickness is equal to $0.04d_j$ in these simulations. The inlet velocity is free of any synthetic turbulence. The Reynolds number is $50,000$, the Mach number is 1.0, and the ratio between the stagnation pressure measured in the jet plenum and the ambient pressure (NPR) is 3.4.

An in-house developed high-fidelity LES parallel code that has been tested and validated in previous studies [17, 8] is used to solve the filtered partial differential equations with the subgrid scale terms being computed using Germano's dynamic model with the adjustment proposed by [13]. A sixth-order central finite difference method is applied in the smooth regions in the spatial directions while a fifth-order weighted essentially non-oscillating scheme with local Lax-Friedrichs flux splitting is used in the discontinuous regions. The temporal integration is performed using a fourth-order five-step Runge-Kutta scheme [11]. The locally one-dimensional inviscid compressible boundary condition proposed by [14] is employed at the outflow boundaries. In addition, a sponge region is employed near the outflow boundaries to minimise the reflections from the outflow boundaries.

Framework of the receptivity analysis

Using the mean flow fields obtained from temporal averaging of the LES results, the linearised Navier Stokes are solved with the same LES resolution in a smaller domain in the radial direction. A sixth-order central finite difference method and fourth-order five-step Runge-Kutta are used for the spatial discretisation and temporal integration, respectively [17, 10]. The forcing is an acoustic initial pressure pulse described by,

$$p'_{@(t=0)} = A\,exp\left(-\frac{(x-x_o)^2}{2\sigma_x^2}-\frac{(r-r_o)^2}{2\sigma_r^2}\right)\cos(2\pi m\theta), \quad (9)$$

where 'A' is the amplitude of the pulse; x_o and r_o are the streamwise and radial location of the centre of the pulse, respectively; σ_x and σ_r are the radii of the pulse in the streamwise and radial directions, respectively. m is the azimuthal mode. To study the sensibility of the pulse location on amplification of the incoming wave by nozzle lip, the centre of the initial pulse is located with a radius of $R_p = 0.4h$ from the nozzle lip and an angle of θ_p from jet axis. This corresponds to the location of the pulse in the axial and the radial directions as $x_o = R_p\sin(\theta_p)$ and $r_o = R_p\cos(\theta_p)$. Detail of the configuration is presented in figure 1.

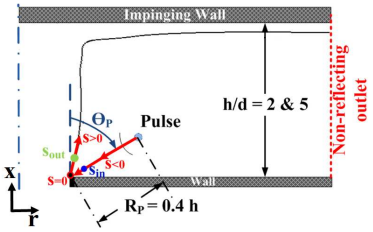

Figure 1: Schematic of the impinging jet with relevant parameters of the receptivity analysis (pulse is located with in a radius of $R_p = 0.4h$ from the nozzle and angle of θ_p from jet axis.).

Table 1: Numerical and physical parameters of the receptivity analysis

Radius of the pulse location (R_p)	$0.4h$
Angular position of the pulse (θ_p)	10° - 85°
The radii of the pulse in the streamwise (σ_x)	$0.05d$
The radii of the pulse in the radial direction (σ_r)	$0.05d$
Amplitude of the pulse (A)	$0.01P_{atm}$
Input location on the s coordinate (s_{in})	$-0.07d$
Output location on the s coordinate (s_{out})	$0.06d$
Azimuthal mode (m)	$0,1,2$

The receptivity analysis tries to quantify the system response to external forcing. In this study, internalisation of the acoustic waves into shear layer instability by the nozzle lip. The nozzle lip acts as an amplifier and hence the process is considered to be linear. Therefore, the linearised Navier Stokes equations is used to study the receptivity process in this concept. The mean flow field is an input for the linearised Navier Stokes equations (equations 1, 2 and 3) which is obtained from the ensemble average of flow field over 38 acoustic time units of the LESs' data. The linearised Navier Stokes are solved to obtain the time evolution of the imposed initial pressure disturbance as a monopole acoustic source. To obtain a better understanding of the receptivity and its sensibility to acoustic pulse location, the transfer function between the input and output energy of the disturbance is calculated. The input is located on the straight line connecting the source to the nozzle lip (blue dot marked as s_{in} in figure 1) and output is located on the shear layer of the jet with a small distance from the nozzle lip (green dot marked as s_{out} in figure 1). A new one-dimensional coordinate is defined as s. It is centred at nozzle lip marked by $s = 0$ in figure 1. Any location on the straight line from the nozzle lip to the acoustic source has a negative sign increasing towards the source location ($s < 0$) and any location on the shear layer has a positive sign in this coordinate which is increasing as distanced from the nozzle lip ($s > 0$). The transfer function is defined in the frequency domain as

$$G(St) = \frac{\hat{E}_{out}(St)}{\hat{E}_{in}(St)}, \quad (10)$$

where St is the Strouhal number, $\hat{E}$ is the Fourier transform of fluctuations of the density weighted total energy of the flow and subscribes *in* and *out* are input and output locations, respectively. The fluctuations of the density weighted total energy, E, is defined as $E = \rho e - \overline{\rho e}$. The parameter values chosen for the analysis are listed in table 1.

The angular position of the initial pulse is varied from near to the impinging wall ($\theta_p = 10^\circ$) to near to the infinite lip ($\theta_p = 85^\circ$) with an incrementation of 5°. The analysis is also

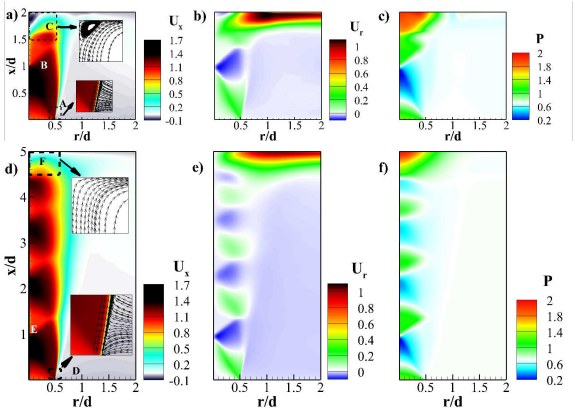

Figure 2: Ensemble averaged a, d) streamwise velocity, b, e) radial velocity and c, f) pressure for nozzle to wall distances of 2d (a-c) and 5d (d-f).

limited to the first three azimuthal modes as they are dominant modes (Not shown here.). To obtain a representative form of the transfer function for the receptivity process then $s_{in} \to 0$ and $s_{out} \to 0$. However the minimum values of s_{in} and s_{out} are limited by the ability to distinguish the input and output signals at the sample points which in turn is limited by the spatial width of the initial acoustic wave and grid resolution in the simulation. Therefore, the values of $s_{in} = 0.07$ and $s_{out} = 0.06$ are selected in this analysis to fulfil these constrains.

Results and discussion

The characteristics of the mean flow is discussed first before moving to the receptivity analysis. Figure 2 presents the contour plots of the time-averaged axial and radial velocities as well as time-averaged pressure fields for the nozzle-to-wall distances of 2d (a-c) and 5d (d-f). The ensemble average of non-dimensionalised variable ϕ is computed as simultaneous temporal and azimuthal means,

$$\bar{\phi}(x,r) = \frac{1}{N_t \times N_\theta} \sum_{i=1}^{N_t} \sum_{j=1}^{N_\theta} \phi(x,r,\theta_j,t_i), \qquad (11)$$

where N_t is the number of datasets over which the average is computed and N_θ is the number of azimuthal grids.

Figure 2a and d show the mean streamwise velocities. The streamlines are shown in zoomed sub-frame near the nozzle exit and the impinging wall. The initial expansion of the shear layer upon exit from the nozzle is clearly visible for both nozzle-to-wall distances. There is a high level of entrainment near the nozzle at region marked by 'A' and 'D'. It is more clear in the zoomed sub-frame where the streamlines are visualised. A small Mach disk with a size of 0.1d is also noticed at $x/d \approx$ 1.0 (marked a 'B' and 'E'). The small size of the Mach disk is due to the low NPR of 3.4. Other classical features of a supersonic under-expanded jet such as a triple point and an oblique shock are also visible. A clear expansion and contraction of the jet boundary is also observed which is a characteristic of under-expanded jets. Upon impingement, a recirculation bubble is observed (labeled as 'C') for the nozzle-to-wall distance of 2d while there is no evidence of the recirculation zone for the nozzle-to-wall distance of 5d (labeled as 'E'). This is more clear in the streamlines of the flow field in this region as presented in the zoomed sub-frame. The contour maps of the radial velocity are presented in figures 2b and e. The triple point and oblique shock are easy to perceive in these plots. The negative mean radial velocity in the region outside of the jet confirms the presence of entrainment. The formation of a strong wall jet at the

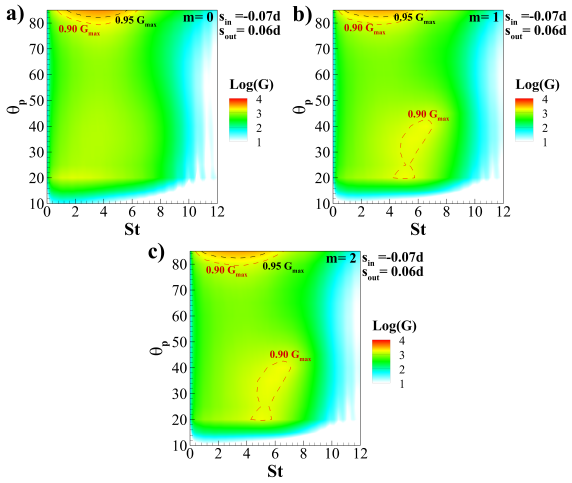

Figure 3: Contour of the logarithm of the transfer function, G, for the nozzle-to-wall distance of 2d for azimuthal mode numbers a) m = 0, b) m = 1 and c) m = 2 (The 90 and 95 percent of the maximum value of the transfer function is marked with red and black dashed lines, respectively.).

impinging wall is visualised. The mean pressure fields are presented in figures 2c and f. There is a pressure drop before the Mach disk. There is also high-pressure region at impingement as the flow is stagnated and a stand-off shock is formed. The modulation of pressure fields can be seen in both cases; however, it is stronger for the shorter nozzle-to-wall distance.

Moving on to receptivity analysis, the transfer function G for the nozzle-to-wall distance of 2d is presented in figure 3 for azimuthal wave-numbers of a) 0, b) 1 and c) 2. The 90 and 95 percent of the maximum value of the transfer function is shown with red and black dashed lines, respectively. The contour level is logarithmic to facilitate the discussion. This is clear that the most amplification of the input signal occurs when the source is located in vicinity of the infinite lip in all three azimuthal modes for the Strouhal numbers in the range of 0.5 to 6.2 with maximum value of the transfer function occurs at St = 3.0. Moving the source location towards the jet centreline, less sensitivity of transfer function to location of the source for the angle between 45° and 75° is observed while the Strouhal number dependency still hold with the Strouhal number of the maximum transfer function shows nearly no dependency on the variation of the source location. On the other hand, the behaviour is different in angles in the ranges of 25° to 45°. The Strouhal number of the maximum transfer function shows no dependency to changes in the location of the pulse for the symmetric pulse (i.e. m = 0) while it moves towards high Strouhal numbers for other two azimuthal modes. A more striking behaviour observed for all azimuthal mode of study when the pulse source is located in θ_p less than 20°. The transfer function is lowest compare to other θ_p angles and dropped significantly as location moves towards the jet shear layer. The maximum amplification of the input signal (i.e. maximum of transfer function) occurs in very low Strouhal numbers as low as 0.2 which is clearer for the symmetric azimuthal mode at θ_p = 10.

Moving to the nozzle-to-wall distance of 5d, the transfer function G for this nozzle-to-wall distance is presented in figure 4 for azimuthal wave numbers a) 0, b) 1 and c) 2. The 90 and 95 percent of the maximum value of the transfer function is shown with red and black dashed lines, respectively. The contour level is same as figure 3. The response to changing the disturbance location is different now. The transfer function is much narrower in frequency domain but is more sensitive in changing the angle from the jet axis, e.i. θ_p. The transfer function shows the maxi-

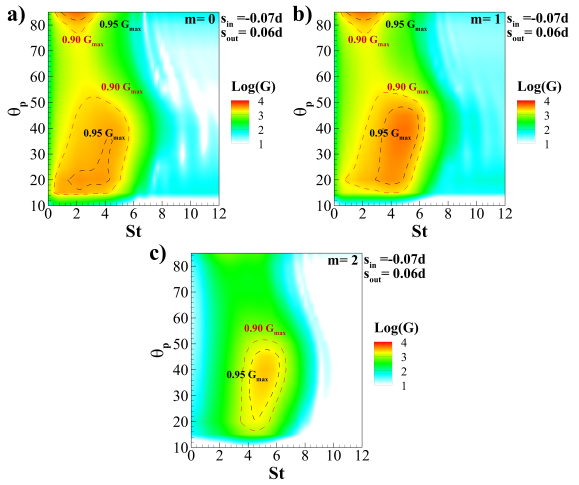

Figure 4: Contour of the logarithm of the transfer function, G, for the nozzle-to-wall distance of $5d$ for azimuthal mode numbers a) m = 0, b) m = 1 and c) m = 2 (The 90 and 95 percent of the maximum value of the transfer function is marked with red and black dashed lines, respectively.).

mum amplification of the input signal in the first two azimuthal mode numbers of 0 (axisymmetric mode) and 1 (helical mode) at both near the infinite lip and $15^\circ < \theta_p < 50^\circ$ while for the azimuthal mode number of 2, the transfer function is maxima when θ_p is in the range of 15° and 50° in contrast to the nozzle-to-wall distance of $2d$ where the maxima is in the regions close to the infinite lip.

Conclusions

The receptivity process at the nozzle-lip to external forcing in the under-expanded supersonic impinging jets has been studied. The instantaneous flow fields are obtained from large eddy simulations for two nozzle-to-wall distances of $2d$ and $5d$. The receptivity has been characterised by a transfer function.This transfer function is defined as the ratio of the output signal to the input signal. The linearised three-dimensional Navier Stokes equations are solved with a near field pressure pulse as an initial condition. The time evolution of the total energy of the disturbances are used at input and output locations to calculate the transfer function. The sensitivity of the transfer function to the pulse location and azimuthal wave number have been performed. It has been demonstrated that the nozzle lip has the highest transfer function when the acoustic sources are located near the infinite lip. This is consistent for the first azimuthal modes of both nozzle-to-wall distances except the m = 2 of the nozzle-to-wall distance of $5d$. It has been also noted that the transfer function is high for the nozzle-to-wall distance of $5d$ when the acoustic forcing is in the region half way between the infinite lip nozzle and the shear layer (i.e. angle between 15° and 50°). Based on these findings, it is suggested that the focus should be on the infinite lip and near reflective surfaces to propose control scenario for these systems.

Acknowledgements

This work was supported by the Australian Research Council. The research benefited from computational resources provided through the National Computational Merit Allocation Scheme, supported by the Australian Government. The computational facilities supporting this project included the Australian NCI Facility, the partner share of the NCI facility provided by Monash University through a ARC LIEF grant and the Multimodal Australian ScienceS Imaging and Visualisation Environment (MASSIVE).

References

[1] Amili, O., Edgington-Mitchell, D., Honnery, D. and Soria, J., Interaction of a supersonic underexpanded jet with a flat plate, in *Fluid-Structure-Sound Interactions and Control*, Springer, 2016, 247–251.

[2] Bechert, D., Excitation of instability waves in free shear layers. part 1. theory, *J. Fluid Mech.*, **186**, 1988, 47–62.

[3] Bechert, D. and Stahl, B., Excitation of instability waves in free shear layers part 2. experiments, *J. Fluid Mech.*, **186**, 1988, 63–84.

[4] Gojon, R., Bogey, C. and Marsden, O., Large-eddy simulation of underexpanded round jets impinging on a flat plate 4 to 9 radii downstream from the nozzle, *AIAA Paper*, **2210**, 2015, 2015.

[5] Henderson, B., Bridges, J. and Wernet, M., An experimental study of the oscillatory flow structure of tone-producing supersonic impinging jets, *J. Fluid Mech.*, **542**, 2005, 115–137.

[6] Ho, C.-M. and Nosseir, N. S., Dynamics of an impinging jet. part 1. the feedback phenomenon, *J. Fluid Mech.*, **105**, 1981, 119–142.

[7] Jones, D. and Morgan, J., The instability of a vortex sheet on a subsonic stream under acoustic radiation, in *Mathematical Proceedings of the Cambridge Philosophical Society*, Cambridge University Press, 1972, volume 72, 465–488, 465–488.

[8] Karami, S., Edgington-Mitchell, D. and Soria, J., Large eddy simulation of supersonic under-expanded jets impinging on a flat plate, in *Proceedings of the 11th Australasian Heat and Mass Transfer Conference*, 2018, 12, 12.

[9] Karami, S. and Soria, J., Analysis of coherent structures in an under-expanded supersonic impinging jet using spectral proper orthogonal decomposition (SPOD), *Aerospace*, **5**, 2018, 1–16.

[10] Karami, S., Stegeman, P. C., Theofilis, V., Schmid, P. J. and Soria, J., Linearised dynamics and non-modal instability analysis of an impinging under-expanded supersonic jet, in *Journal of Physics: Conference Series*, IOP Publishing, 2018, volume 1001, 012019, 012019.

[11] Kennedy, C. A., Carpenter, M. H. and Lewis, R. M., Low-storage, explicit runge–kutta schemes for the compressible navier–stokes equations, *Appl. Numer. Math.*, **35**, 2000, 177 – 219.

[12] Kerschen, E., Receptivity of shear layers to acoustic disturbances, in *Theroretical Fluid Mechanics Conference*, 1996, 2135, 2135.

[13] Lilly, D. K., A proposed modification of the germano subgrid-scale closure method, *Phys. Fluids A: Fluid Dynamics*, **4**, 1992, 633–635.

[14] Poinsot, T. and Lele, S. K., Boundary conditions for direct simulations of compressible viscous flows, *J. Comput. Phys.*, **101**, 1992, 104 – 129.

[15] Powell, A., The sound-producing oscillations of round underexpanded jets impinging on normal plates, *The Journal of the Acoustical Society of America*, **83**, 1988, 515–533.

[16] Raman, G. and Srinivasan, K., The powered resonance tube: from hartmann's discovery to current active flow control applications, *Progress in Aerospace Sciences*, **45**, 2009, 97–123.

[17] Stegeman, P. C., Pérez, J. M., Soria, J. and Theofilis, V., Inception and evolution of coherent structures in under-expanded supersonic jets, in *Journal of Physics: Conference Series*, 2016, volume 708, 012015, 012015.

[18] Tam, C., Excitation of instability waves by sound —a physical interpretation, *Journal of Sound and Vibration*, **105**, 1986, 169 – 172.